Intermetallics 18 (2010) 1185–1196

Contents lists available at ScienceDirect

Intermetallics

journal homepage: www.elsevier.com/locate/intermet

Thermodynamic assessment of the Al–Mo system and of the Ti–Al–Mo System from 0 to 20 at.% Ti

Damian M. Cupid [a,*], Olga Fabrichnaya [a], Fereshteh Ebrahimi [b], Hans J. Seifert [a]

[a] Institute of Materials Science, Technische Universität Bergakademie Freiberg, Freiberg, Germany
[b] Department of Materials Science, University of Florida, Gainesville, Florida, USA

ARTICLE INFO

Article history:
Received 20 January 2010
Received in revised form
1 March 2010
Accepted 3 March 2010
Available online 2 April 2010

Keywords:
A. trialuminides, $TiAl_3$, $NbAl_3$, etc.
E. phase diagram, prediction, including CALPHAD

ABSTRACT

A re-assessment of the thermodynamic description of the binary Al–Mo and of the ternary Ti–Al–Mo system from 0 to 20 at.%Ti was performed. The new Al–Mo description reproduces a congruent melting of the AlMo phase and the calculated phase diagram is in excellent agreement with the experimental data on the Al-rich region showing the formation of several Al-rich intermetallic phases. The new Al–Mo description was used as the constituent binary in the Ti–Al–Mo system and the thermodynamic parameters of the η, β, and δ phases were re-optimized. Calculations using the new description are in good agreement with experimental work performed in the region from 0 to 20 at.% Ti showing the extension of the β phase from the Ti–Mo binary to the Al–Mo binary, the β phase solidification of several alloys, and the transition reaction between the β, Al_8Mo_3, δ, and η phases at 1540 K.

© 2010 Elsevier Ltd. All rights reserved.

1. Introduction

γ-TiAl based alloys are attractive turbine blade materials because they combine a low density ($\approx 4\ g\ cm^{-3}$ [1]) with promising high temperature strength, creep resistance, and oxidation resistance. Various works have shown that the type of microstructure strongly impacts the properties of these alloys [2–5]. Two-phase alloys with submicron-sized, disconnected σ-Nb_2Al precipitates in a γ-TiAl(Nb) matrix are particularly promising as they are expected to exhibit good high temperature creep properties [6,7] and because additions of refractory elements such as Nb have been shown to improve the creep resistance as well as room temperature ductility of γ-TiAl [8–11]. Microstructural control of these alloys can be improved by quenching and retaining the β-bcc single phase solid solution at room temperature to produce the γ-TiAl + σ-Nb_2Al microstructures on aging. To improve the quenchability of the β phase, β stabilizers such as Mo [12, 13] may be used. Since the Ti–Al–Mo system is a subset of the Ti–Al–Nb–Mo system of interest, phase equilibria in the Ti–Al–Mo system should also be investigated to help understand the effect of Mo additions on β phase stabilization.

A thermodynamic description of the Ti–Al–Mo system was developed by Saunders [14] through combination and extrapolation of the Ti–Al, Ti–Mo, and Al–Mo binaries into the ternary. However, calculations using this dataset cannot reproduce the phase equilibria determined by Nino et al. [15] such as: (1) the continuity of the β phase to the Al–Mo binary at 1773 K and 50 at.% Al, (2) the β phase solidification of several alloys with Ti compositions from 15 at.% Ti to 17 at.% Ti and Al compositions from 47 at.% Al to 50 at.% Al, and (3) the transition reaction $\beta + Al_8Mo_3 \rightarrow \delta + \eta$ at 1540 K. In fact, the calculations show that such phase equilibria can only be reproduced if the AlMo phase in the Al–Mo binary melts congruently [16]. This result confirms the experimental work of Rexer [17], who showed the congruent melting of AlMo by metallographic investigation and thermal analysis of various alloys in the Al–Mo system. However, the thermodynamic descriptions of the Al–Mo system from Saunders [14,18] and Du et al. [19] result in the peritectic formation of the AlMo phase from the liquid and δ-$AlMo_3$ phases.

Based on the above discussion, a thermodynamic description for the binary Al–Mo system should be developed which reproduces the congrent melting of the AlMo phase, and this new description should be incorporated into the existing description of the Ti–Al–Mo system [14] to reproduce the phase equilibria from 0 to 20 at.% Ti.

2. Review of the Al–Mo system

The stable phases in the Al–Mo system are included in Table 1. The Al-rich region of the Al–Mo system is characterized by a series of intermetallic phases which form by a cascade of peritectic reactions. The crystal structure and lattice parameters of $Al_{12}Mo$,

* Corresponding author.
E-mail address: damian.cupid@iww.tu-freiberg.de (D.M. Cupid).

0966-9795/$ – see front matter © 2010 Elsevier Ltd. All rights reserved.
doi:10.1016/j.intermet.2010.03.010

Table 1
Stable solid phases in the Ti–Al–Mo system.

Phase	Prototype	Pearson symbol	Space group
$Al_{12}Mo$	WAl_{12}	cI26	$Im\bar{3}$
$Al_5Mo(r)$	–	hP36	$R\bar{3}c$
$Al_5Mo(h_1)$	–	hP60	$P\bar{3}$
$Al_5Mo(h_2)$	WAl_5	hP12	$P6_3$
$Al_{22}Mo_5$	–	oF216	$Fdd2$
$Al_{17}Mo_4$	–	mC84	$C2$
Al_4Mo	WAl_4	mC30	Cm
$Al_{3+x}Mo_{1-x}$	WO_3	cP8	$Pm3n$
$Al_3Mo(h)$	Cr_3Si	mC32	Cm
Al_8Mo_3	–	mC22	$c2/m$
$Al_{63}Mo_{37}$	–	–	–
AlMo	W	cI2	$Im\bar{3}m$
δ-$AlMo_3$	Cr_3Si	cP8	$Pm\bar{3}n$
β	W	cI2	$Im\bar{3}m$
β_0	CsCl	cP2	$Pm\bar{3}m$
α	Mg	hP2	$P6_3/mmc$
α_2-Ti_3Al	Ni_3Sn	hP8	$P6_3/mmc$
γ-TiAl	AuCu	tP2	$P4/mmc$
ε-$TiAl_2$	Ga_2Hf	tI24	$I4_1/amd$
η-(Ti,Mo)Al_3	Al_3Ti	tI8	$I4/mmm$
ζ-Ti_5Al_{11}	Al_3Zr	tI16	$I4/mmm$
(Al)	Cu	cF4	$Fm\bar{3}m$
σ-$Ti_{1.5}Al_2Mo_{1.5}$	σ-CrFe	tP30	$P4_2mnm$

which is the most Al-rich intermetallic phase, were determined by Adam and Rich [20] and Walford [21]. $Al_{12}Mo$ was also confirmed in the works of Sperner [22], Clare [23], Pötzschke and Schubert [24], and Kamei [25] and its peritectic formation temperature was measured at 973 K [22], 976 K [23], and 957 K [25], respectively.

Yamaguchi and Simizu [26] were the first to observe the hexagonal Al_5Mo phase, which was later confirmed in the works of Sperner [22], Pötzschke and Schubert [24], and Kamei et al. [25]. The peritectic formation of Al_5Mo was measured at 976 K [26], 1008 K [22], and 990 K [25], respectively.

The Al_4Mo phase was first mentioned in the work of Wöhler and Michel [27] and was included in the partial Al–Mo phase diagram of Reimann [28]. Reimann [28] confirmed the peritectic formation of Al_4Mo through microstructural investigation of a 12 wt.%Mo as-cast alloy and, using DTA, measured its peritectic formation temperature as 1008 K. Sperner [22], Pötzschke and Schubert [24], and Leake [29] later confirmed the existence of Al_4Mo and Leake [29] gave its crystal structure. Pötzschke and Schubert [24] found the Al_4Mo phase to be stable only at temperatures above 973 K.

Based on microstructural investigation, x-ray diffraction results, and thermal analysis measurements of alloys with Mo contents from 20 to 95 at.%Mo which were heat treated and quenched, Sperner [22] presented the first complete Al–Mo phase diagram. In addition to the $Al_{12}Mo$, Al_5Mo, and Al_4Mo phases, the tetragonal Al_3Mo phase and the Al_2Mo phase were included. Al_3Mo was shown to form peritectically at 1403 K and Al_2Mo was shown to melt congruently at ≈2323 K.

Pötzschke and Schubert [24] changed the stoichiometry of Al_2Mo to Al_8Mo_3 and determined its crystal symmetry to be monoclinic, which was confirmed by Forsyth and Gran [30]. However, Forsyth and Gran [30] incorrectly identified tetragonal Al_3Mo and monoclinic Al_8Mo_3 as the same phase with a homogeneity range from 68.7 to 75 at.%Al. Rexer [17], using EPMA measurements of Al–Mo diffusion couples which were heat treated at 1873 K, 1773 K, and 1673 K and quenched, could not confirm the 68.7 at.%Al composition of the Mo-rich boundary of Al_8Mo_3 suggested by Forsyth and Gran [30].

Pötzschke and Schubert [24] found two additional phases in the composition range from 80 to 83 at.%Al. One phase was identified as a stacking variant of Al_5Mo and the second phase had a complex diffraction pattern which was not analyzed. Van Tenderloo et al. [31] later clarified the stoichiometry of these phases as $Al_{17}Mo_4$ and $Al_{22}Mo_5$, respectively.

The Al-rich liquidus was measured by Yamaguchi and Simizu [26], Yeremenko et al. [32], and Malinovskii [33] at temperatures up to 1273 K. The results of the works are in good agreement with each other. The Al solvus was measured by Röntgen and Koch [34] and Vigdorovich et al. [35], which are also in good agreement with each other.

Phase equilibria at Mo compositions higher than that of Al_8Mo_3 were studied by Ham [36], Ham and Herzig [37], Rexer [17], and Shilo and Franzen [38]. The Mo-rich β solvus was measured at temperatures between 1477 K and 2423 K by Ham and Herzig [37], at 1773 K, 1873 K, and 1973 K by Rexer [17], and at various temperatures between 1845 K and 2021 K by Shilo and Franzen [38]. The results of the β solvus measurements from the respective investigators are in good agreement with each other. The homogeneity range of the δ-$AlMo_3$ phase was measured by Rexer [17] and Shilo and Franzen [38] at the respective temperatures listed above. Ham and Herzig [37] estimated the peritectic formation of the δ-$AlMo_3$ phase at ≈2423 K.

The Al_8Mo_3–Mo region of the phase diagram was investigated by Rexer [17] by thermal analysis and metallographic investigation of several as cast and heat treated and quenched alloys. He found the congruent melting of AlMo, its eutectoid decomposition at 1733 K to Al_8Mo_3 and δ-$AlMo_3$, the eutectic reaction between liquid, AlMo, and δ-$AlMo_3$ phases at ≈ 1993 K, the peritectic formation and eutectoid decomposition of the $Al_{63}Mo_{37}$ phase at 1843 K and 1763 K respectively, and the eutectic reaction between the liquid, Al_8Mo_3, and $Al_{63}Mo_{37}$ phases. In this work, AlMo was shown to have the W-A2 crystal structure.

Based on the above literature, critical evaluations of the phase equilibria in the Al–Mo system were performed by Brewer et al. [39] and Saunders [18]. Walford [40] presented an evaluation of the partial Al–Mo diagram from 0 to 30 at.%Mo. Some aspects of the evaluations are inconsistent with each other and with the literature. Walford [40] modified the partial Al–Mo phase diagram of Sperner [22] by changing the stoichiometry of the Al_3Mo phase to Al_8Mo_3 in accordance with the recommendation of Forsyth and Gran [30], and added the Al_4Mo phase as detected by Pötzschke and Schubert [24]. Walford [40] also modified the composition of the Al_7Mo phase, which was found by Clare [23] in slow cooled melts of Al-rich alloys, to Al_6Mo. However, neither the Al_7Mo phase nor the Al_6Mo phase was confirmed by other authors. Walford [40] then attributed the peritectic formation of Al_3Mo at 1403 K from Sperner [22] to the peritectic formation of the Al_4Mo phase at 1403 K. Although Pötzschke and Schubert [24] indicated that the Al_4Mo phase is stable only above 973 K, Walford [40] showed the Al_4Mo phase existing down to room temperature. The evaluation of Brewer et al. [39] accepted the Al-rich region from Walford [40] but added the peritectic formation of the $Al_{17}Mo_4$ and $Al_{22}Mo_5$ phases of Pötzschke and Schubert [24]. The evaluation of Saunders [18] shows the Al_4Mo phase existing down to room temperature, removes the Al_6Mo phase, and assigns a homogeneity range to the Al_8Mo_3 phase from ≈25 to 31.5 at.%Mo in accordance with the work of Forsyth and Gran [30]. Therefore, although Pötzschke and Schubert [24] showed that Al_8Mo_3 is the correct stoichiometry for the Al_2Mo phase of Sperner [22], the evaluations of Walford [40] and Brewer et al. [39] missed this and replaced the Al_3Mo phase with Al_8Mo_3. The evaluation of Brewer et al. [39] accepted the work of Rexer [17] on the Mo-rich region.

Based on the inconsistencies in the Al-rich region of the Al–Mo system, Schuster and Ipser [41] completely reinvestigated the area from Al to Al_8Mo_3 through microstructural analysis of 15 alloys ranging in composition from 12 to 28 at.%Mo which were heat

treated at temperatures ranging from 873 K for 240 h to 1493 K for 3 h and quenched. Thermal analysis was also performed to measure phase transformation temperatures. The partial Al–Mo phase diagram of Schuster and Ipser [41] shows the $Al_{12}Mo$ phase, which melts incongruently at 985 K, three modifications of the Al_5Mo phase with the high temperature modification melting incongruently at 1119 K, the $Al_{22}Mo_5$ phase which forms peritectically at 1273 K and undergoes eutectoid decomposition at 1104 K, and the $Al_{17}Mo_4$ phase which forms peritectically at 1307 K and exists down to room temperature. These phases are all given as line compounds. The Al_4Mo phase, which melts incongruently at 1450 K and undergoes eutectoid decomposition at 1215 K, was shown to exist over a homogeneity range that extends to higher Mo compositions. The Al_3Mo phase was confirmed by Schuster and Ipser [41] and is shown to form peritectically at 1495 K and undergoes eutectoid decomposition at 1091 K. A new phase, identified as $Al_{3+x}Mo_{1-x}$ with $0 \leq x \leq 0.2$, was found which has the same crystal structure as δ-$AlMo_3$. This phase was shown to exist over the temperature range from 1427 K to 1533 K. Schuster and Ipser measured the congruent melting of the Al_8Mo_3 phase as 1828 ± 10 K. Based on these results, Schuster [42] published a critical assessment of the Al–Mo system in which the Al-rich region was taken from the work of Schuster and Ipser [41] and the Mo-rich region was accepted from Rexer [17]. However, in the critical assessment of Schuster [41], the AlMo phase is assigned the CsCl-B2 structure although Rexer [17] assigned the W-A2 structure based on the x-ray diffraction pattern.

The most recent experimental work on the Al to Al_8Mo_3 region was performed by Eumann et al. [43]. The microstructures of nine binary alloys, which were heat treated at various temperatures between 873 K and 1473 K and quenched, were analyzed. Thermal analysis was also performed to measure phase transformation temperatures. The $Al_{22}Mo_5$ phase was found to exist down to room temperature and the Al_3Mo phase was found to exist to temperatures slightly lower than 1091 K, which was originally given in the work of Schuster and Ipser [41]. The congruent melting of Al_8Mo_3 was measured as 1819 ± 3 K, which is in good agreement with the work of Schuster and Ipser [41]. According to Eumann et al. [43], all investigated phases exhibited a homogeneity range between 0.1 and 0.4 at.%Mo. Eumann et al. [43] also gave tie line data for the δ-$AlMo_3 + Al_8Mo_3$ equilibrium at 1073 K, 1273 K, and 1473 K. The presence of the $Al_{3+x}Mo_{1-x}$ phase was not confirmed.

Experimental thermodynamic data on the Al–Mo system are available from Shilo and Fanzen [38], Meschel and Kleppa [44], and Sudavtsova et al. [45]. Shilo and Fanzen [38] used vapor pressure measurements from the Knudsen effusion method to calculate the enthalpies of formation of the Al_8Mo_3, AlMo, δ-$AlMo_3$ phases and of the Mo-rich β solid solution at 89, 92, 96, and 98 at.%Mo. Additionally, Meschel and Kleppa [44] used direct reaction calorimetry to measure the enthalpies of formation of the δ-$AlMo_3$ and Al_8Mo_3 phases, and Sudavtsova et al. [45] measured the enthalpies of mixing of the liquid at 5, 10, 15, and 18 at.%Mo.

Two thermodynamic descriptions for the Al–Mo system were developed by Saunders [18,14]. In both descriptions, the AlMo phase forms peritectically from the liquid and δ-$AlMo_3$ phases as Saunders [18,14] could not reproduce the congruent melting of AlMo. The $Al_{17}Mo_4$, $Al_{22}Mo_5$, and Al_3Mo phases in the Al–Al_8Mo_3 region were not considered. Additionally, the δ-$AlMo_3$ phase is modeled as a stoichiometric phase with no homogeneity range. The first dataset of Saunders [18] used an earlier version of the SGTE descriptions for pure Mo and Al [46] and modeled the AlMo and Mo-rich β phases as a single phase. In the second dataset [14], the SGTE descriptions for the pure elements [47] were used, but the AlMo and Mo-rich β phases were modeled as separate phases.

Recently, a new description of the Al–Mo system has been published by Du et al. [19] in which the Al–Al_8Mo_3 region was accepted from Eumann et al. [43]. Although the Mo-rich β phase and the AlMo phase are modeled with the same function, the AlMo phase forms peritectically from the liquid and δ-$AlMo_3$ phases according to the calculations.

3. Phase relations in the Ti–Al–Mo system

The crystallographic data of the solid phases in the Ti–Al–Mo system are given in Table 1. There is no information on the solubility of Ti in the $Al_{12}Mo$, Al_5Mo, $Al_{22}Mo_5$, $Al_{17}Mo_4$, Al_4Mo, and $Al_{63}Mo_{37}$ binary Al–Mo phases, but there is evidence in the literature that the Al_8Mo_3 and δ-$AlMo_3$ phases dissolve Ti. For example, the equilibrium $\beta + Al_8Mo_3 + \delta$-$AlMo_3$ tie-triangle data for an alloy of composition 3 at.%Ti–52 at.%Al–45 at.%Mo, which was heat treated at 1673 K and quenched, showed that the Al_8Mo_3 phase dissolved 1 at.%Ti and that the δ-$AlMo_3$ phase dissolved 2.7 at.%Ti [15]. Additionally, an alloy of composition 18 at.%Ti–24 at.%Al–58 at.% Mo, which was heat treated at 1198 K and quenched, contained only the δ-$AlMo_3$ phase [48], which indicates that the δ-$AlMo_3$ phase extends to at least 18 at.%Ti at 1198 K in the Ti–Al–Mo system.

The η-(Ti,Mo)Al_3 phase, which is based on the binary $TiAl_3$ phase, exists over a large homogeneity range in the ternary Ti–Al–Mo system. Hansen and Raman [48] showed that alloys of composition 26 at.%Ti–64 at.%Al–10 at.%Mo, 16 at.%Ti–68 at.% Al–16 at.%Mo, and 12.5 at.%Ti–75 at.%Al–12.5 at.%Mo were all single phase η-(Ti,Mo)Al_3 at 1198 K, and the η-(Ti,Mo)Al_3 phase was found to extend to Mo compositions as high as 20 at.%Mo and Al compositions as low as 62 at.%Al at 1198 K [48]. Eremenko et al. [49] confirmed the large homogeneity range of the η-(Ti,Mo)Al_3 phase at 1573 K, and Abdel-Hamid [50] found the η-(Ti,Mo)Al_3 phase containing as much as 9.04 at.%Mo from his work on slow-cooled Al-rich dilute melts. The large extension of the η-(Ti,Mo)Al_3 phase occurs through substitution of Mo on both Al and Ti sites of the $TiAl_3$ structure [48].

Das et al. [12] showed that at 1448 K, the γ-TiAl phase contains $\approx$1 at.%Mo at 52 at.%Ti and $\approx$3 at.%Mo at 48 at.%Ti whereas Morris et al. [3] measured the Mo content of the γ-TiAl phase in equilibrium with the α_2-Ti_3Al and β_0 phases at 1173 K and 1473 K as 1 at.% Mo at 51 at.%Ti and 1.5 at.%Mo at 53 at.%Ti respectively. Kimura and Hashimoto [51] measured the Mo content of the γ-TiAl phase in equilibrium with the α_2-Ti_3Al and β_0 phases at 1473 K as 0.5 at.%Mo at 50 at.%Ti, which is much lower than that measured in the work of Das et al. [12]. However, Das et al. [12] heat treated their alloys for 120 h whereas Kimura and Hashimoto [51] heat treated their alloys for only 4 h. Therefore, the work of Das et al. [12] may more closely give the equilibrium composition of the γ-TiAl phase at 1473 K. Singh and Banerjee [52] showed that the maximum composition of Mo in the γ phase at 1673 K is 3 at.%Mo.

Although the maximum solubility of Mo in the α phase has not been measured, Singh and Banerjee [52] showed that an alloy of composition 50 at.%Ti–48 at.%Al–2 at.%Mo is in the single phase α field at 1673 K and suggested that the α phase field extends to an alloy of composition 44 at.%Ti–50 at.%Al–6 at.%Mo at 1673 K. The Ti-rich α single phase was also observed in an alloy 95 at.%Ti–2.5 at. %Al–2.5 at.%Mo which was heat treated at 1073 K for 222 h and quenched [53].

The solubility of Mo in the α_2-Ti_3Al phase is unclear. Although Banerjee et al. [54] published partial isothermal sections at 1673 K, 1573 K, and 1473 K showing the α_2-Ti_3Al phase, the microstructures of the investigated alloys were interpreted taking into account a description of the binary Ti–Al phase diagram from Margolin [55] which showed the peritectic formation of α_2-Ti_3Al from the liquid

and β phases at 1745 K. However, the critically assessed Ti–Al phase diagram of Schuster and Palm [56] shows the peritectoid formation of the α_2-Ti_3Al phase from the β and α phases at 1473 K. Therefore, it is possible that Banerjee et al. [54] misidentified the α phase as the α_2-Ti_3Al phase. In fact, the partial isothermal sections at 1448 K of Das et al. [57] and at 1573 K and 1473 K of Kimura and Hashimoto [51] show only the α phase. However, Morris et al. [3] claimed to also have the α_2-Ti_3Al phase at 1473 K.

The ordered β_0 phase was first determined by Böhm and Löhberg [58] in alloys within the composition range from ≈60 wt.%Mo to ≈30 wt.%Mo at 50 at.%Ti which were heat treated at 1073 K and then quenched. Singh et al. [59] performed Rietveld refinement of X-ray and neutron diffraction data from an alloy of composition 50 at.%Ti–25 at.%Al–25 at.%Mo which was homogenized at 1273 K and furnace cooled. The alloy was found to contain the β_0 phase, and Rietveld refinement of the data showed that Ti atoms occupy A sites and Al and Mo atoms occupy the B sites in the CsCl structure. Excess Mo atoms can also occupy A sites with Ti atoms [59].

There is one ternary phase in the Ti–Al–Mo system. Hansen and Raman [48] found the ternary σ phase in the single phase alloy of composition 26 at.%Ti–41 at.%Al–33 at.%Mo at 1198 K. The σ phase was found to have a very small homogeneity range and the stoichiometry $Ti_{1.5}Al_2Mo_{1.5}$ was assigned. The presence of the ternary σ phase was confirmed in the work of Eremenko et al. [53]. The σ phase forms through a peritectoid reaction at ≈1523 K [60].

Nino et al. [15] published the most comprehensive work on the phase equilibria in the Ti–Al–Mo system from 0 to 20 at.%Ti. Several samples with Al contents ranging from 45 to 55 at.%Al and Ti contents ranging from 3 to 17 at.%Ti were heat treated at 1773, 1723, and 1673 K and quenched. DTA was also performed to measure solid state transformation temperatures. Based on the results of metallographic analysis and DTA, partial isothermal sections from 0 to 20 at.%Ti at 1673, 1573, 1540, 1473, and 1373 K, as well as an isopleth through 50 at.%Al from 0 to 20 at.%Ti were constructed. It was also concluded that the transition reaction $\beta + Al_8Mo_3 \rightarrow \delta + \eta$ should take place at ≈1540 K. The results of Nino et al. [15] also confirmed that the β phase is continuous in the solid state solution from the Ti–Mo binary to the Al–Mo binary since an alloy of composition 3 at.%Ti–52 at.%Al–45 at.%Mo, with only 3 at.%Ti, showed a single phase β microstructure following heat treatment at 1773 K and quenching [15].

Critical assessments of the phase equilibria in the Ti–Al–Mo system were performed by Budberg and Schmid-Fetzer [61] based on results published up to 1990, Tretyachenko [60] based on results published up to 2003, and Raghavan [62] based on results published up to 2005. Tretyachenko used the assessed Al–Mo diagram from Schuster [42] and the assessed Al–Ti diagram from Schmid-Fetzer [63] as the constituent binaries for the assessment whereas Raghvan [62] used the Al–Mo from Saunders [18], updated to include the experimental work of Schuster and Ipser [41] on the Al–Al_8Mo_3 region, and the Al–Ti system from Raghavan [64]. Both Tretyachenko and Raghavan use the Mo–Ti binary from Massalski [65].

Contrary to the work of Nino et al. [15], the AlMo and β phases were not considered to form a continuous solid solution in the assessment of Tretyachenko [60]. Instead, the assessed 1873 K isothermal section shows a two phase AlMo + β field with a maximum solubility of Ti in AlMo of ≈3 at.%Ti. Tretyachenko [60] considered the AlMo and β phases as separate phases based on the Al–Mo evaluation of Schuster [42] in which the AlMo phase was assigned the CsCl–B2 structure. When the β solidifying alloy of composition 3 at.%Ti–52 at.%Al–45 at.%Mo of Nino et al. [15] is superimposed on the critically evaluated solidus surface of Tretyachenko [60], it is located in the β + AlMo + $Al_{63}Mo_{37}$ three phase field forming from the invariant reaction liquid + AlMo → β + $Al_{63}Mo_{37}$ which, according to Tretyachenko's partial Scheil reaction scheme, takes place at 1823 K. Combining the information available from the assessed 1873 K isothermal section, the information available from the assessed solidus surface, and the partial Scheil reaction scheme, the β solidifying 3 at.% Ti–52 at.%Al–45 at.%Mo alloy would instead solidify as liquid → liquid + AlMo → liquid + AlMo + β → β + AlMo + $Al_{63}Mo_{37}$ and therefore could never exist as single phase β at 1773 K. Ragahavan [62] took into account the experimental work of Nino et al. [15] in his assessment. Therefore, as only partial isothermal sections from 0 to 30 at.%Ti are presented at 1573, 1473, and 1373 K, there is no obvious contradiction with the work of Nino et al. [15].

A thermodynamic description for the Ti–Al–Mo system is available from Saunders [14]. However, calculations performed using this dataset cannot reproduce the results of the experimental work of Nino et al. [15] which indicate the extension of the β phase to the Ti-poor region of the Ti–Al–Mo system and the continuity of the β phase from the Ti–Mo binary to the Al–Mo binary. For example, although the alloy of composition 3 at.%Ti–52 at.% Al–45 at.%Mo should be single phase β at 1773 K [15], this alloy is calculated in the liquid + β + $Al_{63}Mo_{37}$ three phase field at the same temperature and is located in the primary crystallization field of the δ phase on the calculated liquidus surface [16]. Furthermore, the calculated β phase does not extend to high enough Al compositions at sub-solidus temperatures as the four alloys with Ti compositions ranging from 15 to 17 at.%Ti and Al compositions ranging from 47 to 50 at.%Al, which have been shown to be single phase β at 1723 K by Nino et al. [15], are calculated in other phase fields, and the invariant reaction $\beta + Al_8Mo_3 \rightarrow \delta + \eta$ could not be calculated at any temperature [16]. The contradictions between the calculated and experimentally determined phase equilibria result from an insufficient extension of the β phase to very low Ti compositions close to the Al–Mo binary, and are excellent confirmation that the thermodynamic parameters for the Al–Mo system should be re-assessed.

4. Thermodynamic Modeling

The Gibbs energy $G_{AxBy}(T)$ of a stoichiometric phase A_xB_y was modeled as:

$$G_{AxBy}(T) - x^0H^{\phi}{}_A - y^0H^{\phi}{}_B = a + bT + cT\cdot\ln T + dT^2 + eT^3 + fT^{-1} + \ldots \quad (1)$$

which may also be expressed as:

$$G_{AxBy}(T) - x^0H^{\phi}{}_A - y^0H^{\phi}{}_B = \Delta_f G_{AxBy}(T) + x\mathrm{GHSER}_A + y\mathrm{GHSER}_B \quad (2)$$

where ${}^0H_i^{\phi}$ is the enthalpy of pure element i in state ϕ at 298.15 K, $\Delta_f G_{AxBy}(T)$ is the Gibbs energy of formation of the stoichiometric phase from the pure elements, and GHSER_i is the Gibbs free energy of pure element i referred to the enthalpy of its stable state at 298.15 K.

Substitutional solutions were modeled as

$$G_m^{\phi} = G_m^{\phi,\mathrm{srf}} + G_m^{\phi,\mathrm{conf}} + G_m^{\phi,\mathrm{E}} = \sum_i^n x_i^0 G_i^{\phi} + RT\sum_i^n x_i \times \ln x_i + G_m^{\phi,\mathrm{E}} \quad (3)$$

where $G_m^{\phi,\mathrm{srf}} = \sum_i^n x_i^0 G_i^{\phi}$ is the surface of reference term, $G_m^{\phi,\mathrm{conf}} = RT\sum_n x_i \times \ln x_i$ is the Gibbs free energy resulting from the configurational entropy of mixing, and $G_m^{\phi,E}$ is the excess Gibbs free energy of mixing, which was modeled as:

$$G_m^{\phi,E} = G_m^{\phi,bin.E} + G_m^{\phi,tern.E} = \sum_{i=1}^{n-1}\sum_{j=i+1}^{n} x_i x_j {}^{\nu}L_{ij}^{\phi} + \sum_{i=1}^{n-2}\sum_{j=i+1}^{n-1}\sum_{k=j+1}^{n} x_i x_j x_k L_{ijk}^{\phi} \quad (4)$$

where $G_m^{\phi,bin.E}$ and $G_m^{\phi,tern.E}$ represent all binary and ternary interactions, respectively. The binary interaction parameters L_{ij}^{ϕ} were modeled using Redlich–Kister polynomials [66], expressed as:

$${}^{\nu}L_{ij}^{\phi} = \sum_{\nu=0}^{n} {}^{\nu}L_{ij}^{\phi}(x_i - x_j)^{\nu} \quad (5)$$

and the ternary interaction parameters L_{ijk}^{ϕ} were modeled as [67]:

$${}^{\nu}L_{ijk}^{\phi} = x_i \cdot {}^{i}L_{ijk}^{\phi} + x_j \cdot {}^{j}L_{ijk}^{\phi} + x_k \cdot {}^{k}L_{ijk}^{\phi} \quad (6)$$

Solution phases with two or more sublattices in which the composition of at least one of the constituent sublattices is allowed to vary were modeled using the compound energy formalism [68]. The Gibbs energy of a phase using this formalism is expressed as:

$$G_m^{\phi} = G_m^{\phi,srf} + G_m^{\phi,conf} + G_m^{\phi,E} = \sum \Delta_f^0 G_{end} \prod y_i^s + RT \sum_s \sum_i n^s y_i^s \ln y_i^s + G_m^{\phi,E} \quad (7)$$

where $G_m^{\phi,srf} = \sum \Delta_f^0 G_{end} \prod y_i^s$ is the surface of reference term, $G_m^{\phi,conf} = RT \sum \sum_i n^s y_i^s \ln y_i^s$ is the Gibbs free energy resulting from configurational entropy of mixing on each sublattice, and $G_m^{\phi,E}$ is the contribution of the excess Gibbs energy. For the first two terms, $\Delta_f^0 G_{end}$ is the Gibbs energy of formation of the end-members, y_i is the site fraction of species i on sublattice s, and n is the stoichiometric coefficient for each sublattice. The excess Gibbs energy $G_m^{\phi,E}$ was modeled as:

$$G_m^{\phi,E} = \sum_P \prod_{s \neq r} y_i^s \times y_A^r \times y_B^r \times L_{A,B:C} \quad (8)$$

where P represents the condition of an additional constituent on sublattice r while all other sublattices are singularly occupied.

The CALPHAD [69,70] based thermodynamic optimization of the Al–Mo and Ti–Al–Mo systems was performed using the PARROT [71] module of THERMO-CALC [72] and phase diagrams were calculated using either THERMO-CALC or PANDAT [73] software.

5. Thermodynamic optimization of the Al–Mo system

For the optimization of the Al–Mo system, the peritectic formation of δ-$AlMo_3$ was accepted from Ham and Hervig [37], and the phase equilibria between δ-$AlMo_3$ and Al_8Mo_3 were accepted from Rexer [17], i.e., the congruent melting of the AlMo phase and eutectic reaction between liquid, δ-$AlMo_3$, and AlMo. The congruent melting temperature of AlMo was taken from the critical evaluation of Schuster [42]. Phase equilibria in the Al-rich region were accepted from the experimental work of Eumann et al. [43]. Since the homogeneity ranges of the Al-rich intermetallic phases were measured as between 0.1 and 0.4 at.%Mo, they were modeled as stoichiometric phases. The thermodynamic description of Saunders [14] was used as the starting dataset for the re-optimization.

5.1. Optimization strategy

The parameters of the β and the liquid phases were optimized simultaneously to be able to reproduce the congruent melting of AlMo (the β phase at ≈50 at.%Mo), the eutectic reaction between the liquid, β, and δ-$AlMo_3$ phases at ≈1993 K, and the peritectic formation of the δ-$AlMo_3$ phase at ≈2423 K, and to fit the Mo-rich β solvus to the measured values from Ham and Herzig [37], Rexer [17], and Shilo and Franzen [38]. The parameters of the liquid were optimized to fit the experimental data on the enthalpies of mixing of the liquid at 5, 10, 15 and 18 at.%Mo from Sudavtsova et al. [45] and the Al-rich liquidus determined by Yamaguchi and Simizu [26], Yeremenko et al. [32], and Malinovskii [33] at temperatures up to 1273 K. At this step of the optimization, only the Al_8Mo_3 phase in the Al-rich region was considered.

Next, the parameters of the δ-$AlMo_3$ phase were optimized to fit the Al-rich boundary of the δ-$AlMo_3$ phase in equilibrium with Al_8Mo_3 at 1073, 1273, and 1473 K according to the experimental results of Eumann et al. [43]. Afterwards, the Al-rich intermetallic line compounds were successively introduced, starting with Al_3Mo and ending with $Al_{12}Mo$, to reproduce the Al–Al_8Mo_3 region of the phase diagram by Eumann et al. [43]. Following this, the parameters of the (Al) solid solution were re-optimized to fit the data on the (Al) solvus from Röntgen and Koch [34] and Vigdorovich et al. [35]. In the final step, all parameters of all phases were re-optimized simultaneously to reproduce the available experimental data.

5.2. Selection of optimizing parameters

5.2.1. The beta phase

The β phase with W-A2 structure is modeled as a substitutional solution (Al,Mo). In this work, the ${}^0L_{Al,Mo}^{\beta}$, ${}^1L_{Al,Mo}^{\beta}$, and ${}^2L_{Al,Mo}^{\beta}$ parameters were optimized. The ${}^0L_{Al,Mo}^{\beta}$ parameter was modeled as a linear function of temperature whereas the ${}^1L_{Al,Mo}^{\beta}$ and ${}^2L_{Al,Mo}^{\beta}$ parameters were modeled as temperature independent. The ${}^1L_{Al,Mo}^{\beta}$ and ${}^2L_{Al,Mo}^{\beta}$ parameters were required to describe the AlMo and Mo-rich β phases as a single phase.

5.2.2. The liquid phase

The liquid phase is modeled as a substitutional solution (Al,Mo). A third order Redlich–Kister polynomial description for the liquid phase was required to fit the congruent melting of the β phase at 50 at.%Mo, the eutectic reaction between the liquid, β, and δ-$AlMo_3$ phases, and the peritectic formation of the δ-$AlMo_3$ phase. The ${}^0L_{Al,Mo}^{liquid}$, ${}^1L_{Al,Mo}^{liquid}$, ${}^2L_{Al,Mo}^{liquid}$, and ${}^3L_{Al,Mo}^{liquid}$ Redlich–Kister polynomial parameters were modeled as linear functions of temperature.

5.2.3. The Al-rich intermetallic phases

Since the homogeneity ranges of the Al-rich intermetallic phases were measured as between 0.1 and 0.4 at.%Mo by Eumann et al. [43], these phases were modeled as stoichiometric compounds. The Gibbs energy of formation $\Delta_f G_{Al_xMo_y}$ of the intermetallic phase Al_xMo_y was modeled as a linear function of temperature as:

$$\Delta_f G_{Al_xMo_y}(T) = a + bT \quad (9)$$

where the parameters a and b, respectively, give the enthalpy and entropy of formation of Al_xMo_y from the pure elements.

For the Al_8Mo_3 phase, a was assigned a value of −429 kJ, which corresponds to the enthalpy of formation of Al_8Mo_3 calculated using the Third law method from the vapor pressure measurements of Shilo and Franzen [38]. The value of b was assigned to fit the congruent melting of Al_8Mo_3 at 1819 K measured by Eumann et al. [43].

The values of the a and b parameters for Al_3Mo were chosen to reproduce the peritectic formation of Al_3Mo from Al_8Mo_3 and liquid at 1495 K and the eutectoid decomposition of Al_3Mo to Al_8Mo_3 and the higher Al-containing liquid at 1063 K [43]. Similarly, the values of the a and b parameters for Al_4Mo were chosen to reproduce the peritectic formation of Al_4Mo from Al_3Mo and liquid

at 1425 K and the eutectoid decomposition of Al_4Mo to Al_3Mo and the liquid phase with higher Al content.

The $Al_{17}Mo_4$, $Al_{22}Mo_5$, Al_5Mo, and $Al_{12}Mo$ phases exist down to room temperature. Since the Gibbs energy of formation is modeled as a linear function of temperature, the starting values of a and b were generated in a two step procedure. First, $\Delta G_{AlxMoy}(T_P)$, which is the value of the Gibbs free energy of the phase required to reproduce its peritectic formation at the respective temperature T_P was determined. Using the value $\Delta G_{AlxMoy}(T_P)$, a value of b was chosen using trial and error so that the respective phase is stable down to room temperature. The Gibbs energy of the phase as a function of temperature, $G_{AlxMoy}(T)$, could then be defined.

5.2.4. The $AlMo_3$ phase

The δ-$AlMo_3$ phase is modeled using the compound energy formalism as:

$$(Al, Mo^*)_3(Al^*, Mo) \quad (10)$$

where the asterisk identifies the major species on each sublattice. This modeling results in the four end members $G^{\delta}_{Al:Al}$, $G^{\delta}_{Al:Mo}$, $G^{\delta}_{Mo:Al}$, and $G^{\delta}_{Mo:Mo}$. The $G^{\delta}_{Mo:Al}$ end member, which influenced the peritectic formation temperature of the δ-$AlMo_3$ phase from the liquid and Mo-rich β phases, the eutectic reaction between the δ-$AlMo_3$, liquid, and AlMo phases, and the eutectoid decomposition of the AlMo phase to δ-$AlMo_3$ and Al_8Mo_3, was modeled with a linear temperature dependence. Large positive values were assigned to all other end member terms. The binary interaction parameters ${}^0L^{\delta}_{Al,Mo:Al}$ and ${}^0L^{\delta}_{Mo:Al,Mo}$ were found to influence the homogeneity range of δ-$AlMo_3$ phase. These mixing parameters were modeled with a linear temperature dependence and were optimized to fit the Al-rich boundary of the δ-$AlMo_3$ phase at 1073, 1273, and 1473 K to agree with the δ-$AlMo_3 + Al_8Mo_3$ tie line data of Eumann et al. [43], as well as the composition of the δ-$AlMo_3$ phase at the invariant reactions (Table 2) from the evaluation of Schuster [42].

Table 2
Invariant reactions in the Al–Mo system.

Reaction $\varphi_1 + \varphi_2 + \varphi_3$	Temperature [K]	Phase composition [at.%Al]			Reference
		φ_1	φ_2	φ_3	
Liquid + $\beta \rightarrow \delta$-$AlMo_3$	~2423	~30.0	19.5	25.0	[42]
	~2423	–	–	–	[37]
	2423	25.5	21.1	24.5	This work
Liquid → AlMo	2023	50.0	50.0	–	[42]
	2023	48.4	48.4	–	This work
Liquid → δ-$AlMo_3$ + AlMo	~1993	~37.0	~28.5	~46.0	[42]
	~1993	–	–	–	[17]
	1993	43.7	29.2	45.6	This work
Liquid + AlMo → $Al_{63}Mo_{37}$	1843	~66.0	~52.0	~63.0	[42]
	1843	–	–	–	[17]
	1843	63.1	55.3	63.0	This work
Liquid → Al_8Mo_3	1828 ± 10	72.7	72.7	–	[42]
	1819 ± 5	–	–	–	[43]
	1821	72.7	72.7	–	This work
Liquid → $Al_{63}Mo_{37} + Al_8Mo_3$	1808	~71.5	~63.0	72.7	[42]
	1808	–	–	–	[17]
	1819	69.6	63.0	72.7	This work
$Al_{63}Mo_{37} \rightarrow$ AlMo + Al_8Mo_3	1763	~63.0	~50.5	72.7	[42]
	1763	–	–	–	[17]
	1763	63.0	52.0	72.7	This work
AlMo → δ-$AlMo_3 + Al_8Mo_3$	1743	50.0	~27.0	72.7	[42]
	1743	–	–	–	[17]
	1743	50.5	29.1	72.7	This work
Liquid + $Al_8Mo_3 \rightarrow Al_3Mo$	1495	–	–	–	[41, 43]
	1495	95.3	–	–	This work
Liquid + $Al_3Mo \rightarrow Al_4Mo$	1425	–	–	–	[43]
	1425	96.7	–	–	This work
Liquid + $Al_4Mo \rightarrow Al_{17}Mo_4$	<1273	–	–	–	[43]
	1270	99.5	–	–	This work
$Al_4Mo \rightarrow Al_3Mo + Al_{17}Mo_4$	1215	–	–	–	[41, 43]
	1215	–	–	–	This work
Liquid + $Al_{17}Mo_4 \rightarrow Al_{22}Mo_5$	<1223	–	–	–	[43]
	1213	99.4	–	–	This work
Liquid + $Al_{22}Mo_5 \rightarrow Al_5Mo$	1119	–	–	–	[41, 43]
	1119	99.8	–	–	This work
$Al_3Mo \rightarrow Al_8Mo_3 + Al_{17}Mo_4$	<1073	–	–	–	[43]
	1064	–	–	–	This work
Liquid + $Al_5Mo \rightarrow Al_{12}Mo$	985	–	–	–	[41, 43]
	985	99.97	–	–	This work

5.2.5. The (Al) phase

The (Al) solid solution was modeled as a substitutional solid solution (Al,Mo). The ${}^{0}L^{(Al)}_{Al,Mo}$ was optimized to fit the data on the (Al) solvus from Röntgen and Koch [34] and Vigdorovich et al. [35]. This parameter was modeled with a linear temperature dependence.

6. Thermodynamic optimization of the Ti–Al–Mo system

The Ti–Al and Ti–Mo binary descriptions were kept from the original dataset of Saunders [14] and the new Al–Mo description from the present work was adopted. Only the ternary parameters of the η, β, and δ-$AlMo_3$ phases were re-optimized to be able to reproduce the equilibria in the 0–20 at.%Ti region of the Ti–Al–Mo system from Nino et al. [15].

6.1. Optimization strategy

In the first step, the parameters of the η phase were re-optimized to reproduce the transition reaction $\beta + Al_8Mo_3 \rightarrow \delta + \eta$ at 1540 K. Then, the parameters for the β, and η phases were optimized simultaneously to reproduce the $Al_8Mo_3 + \delta + \beta$ three phase triangle at 1673 K and the composition of the β phase in equilibrium with the η and δ phases at 1423 K. Next, the parameters of the δ phase were re-optimized to improve the fit of the composition of the δ phase in the $Al_8Mo_3 + \delta$-$AlMo_3 + \beta$ three phase triangle at 1673 K. Last, the parameters of the β and η phases were re-optimized simultaneously to calculate the solid state transformation temperatures of alloys with 5, 7, 10, 13, 15, and 17 at.%Ti and 50 at.% Al, which were measured using thermal analysis by Nino et al. [15].

6.2. Selection of optimizing parameters

6.2.1. The Eta phase

The η phase, which has the tI8-Al_3Ti structure, is modeled using the compound energy formalism as:

$$(Al*, Mo, Ti)_{0.75}(Al, Mo*, Ti)_{0.25} \quad (11)$$

where the asterisk identifies the major species on each sublattice. The descriptions for the $G^{\eta}_{Al:Ti}$, $G^{\eta}_{Mo:Mo}$, $G^{\eta}_{Mo:Ti}$, $G^{\eta}_{Ti:Mo}$, $G^{\eta}_{Ti:Ti}$, $G^{\eta}_{Al:Al}$, and $G^{\eta}_{Ti:Al}$ end members were accepted from Saunders [14] and the $G^{\eta}_{Al:Mo}$ end member was taken from the re-optimized parameters of the Al–Mo system. The $G^{\eta}_{Mo:Al}$ parameter was given a positive value of +20 kJ/mol. Although Saunders [14] originally included only the ${}^{0}L^{\eta}_{Al,Mo:Mo}$, ${}^{0}L^{\eta}_{Al,Mo:Ti}$, and ${}^{0}L^{\eta}_{Al,Ti:Ti}$ mixing parameters, these parameters were not enough to extend the homogeneity range of the η phase in accordance with the work of Hansen and Ramen [48] and Eremenko et al. [49]. Therefore, additional mixing parameters under the following assumptions:

$${}^{0}L^{\eta}_{Al:Mo:Mo} = {}^{0}L^{\eta}_{Al,Mo:Ti} = {}^{0}L^{\eta}_{Al,Mo:Al} = {}^{0}L^{\eta}_{Al,Mo:*} \quad (12)$$

$${}^{0}L^{\eta}_{Al,Mo:Ti} = {}^{0}L^{\eta}_{Mo:Mo,Ti} = {}^{0}L^{\eta}_{Ti:Mo,Ti} = {}^{0}L^{\eta}_{*:Mo,Ti} \quad (13)$$

$${}^{0}L^{\eta}_{Al,Ti:Ti} = {}^{0}L^{\eta}_{Al,Ti:Al} = {}^{0}L^{\eta}_{Al,Ti:Mo} = {}^{0}L^{\eta}_{Al,Ti:*} \quad (14)$$

were used. The ${}^{0}L^{\eta}_{Al,Mo:Ti} = {}^{0}L^{\eta}_{*:Mo,Ti}$ parameter strongly influenced the $\beta + Al_8Mo_3 \rightarrow \delta + \eta$ invariant equilibrium, and was used to fit the transition temperature to 1540 K.

6.2.2. The beta phase

The β phase, which has the cI2-W structure, is modeled as the substitutional solution (Al, Mo, Ti). Only the ${}^{0}L^{\beta}_{Al,Mo,Ti}$, ${}^{1}L^{\beta}_{Al,Mo,Ti}$, and the ${}^{2}L^{\beta}_{Al,Mo,Ti}$ mixing parameters were optimized with starting values taken from the original dataset of Saunders [14].

6.2.3. The delta phase

The δ phase with cP8-Cr_3Si structure is modeled using the compound energy formalism as:

$$(Al, Mo*, Ti)_{0.75}(Al*, Mo, Ti)_{0.25} \quad (15)$$

The $G^{\delta}_{Ti:Al}$ end member was accepted from the original description of Saunders [14] and the $G^{\delta}_{Mo:Al}$ end member was taken from the new Al–Mo description. All other end member parameters were given a positive value +10 kJ/mol to make them unstable. The ${}^{0}L^{\delta}_{Al,Mo:Al}$ and ${}^{0}L^{\delta}_{Mo:Al,Mo}$ binary mixing parameters were taken from the new Al–Mo description and the ${}^{0}L^{\delta}_{Mo,Ti:Al}$ mixing parameter, which influenced the extension of the δ phase into the ternary, was used to fit the composition of the δ phase in the $Al_8Mo_3 + \delta$-$AlMo_3 + \beta$ three phase triangle at 1673 K from Nino et al. [15].

7. Results and discussion

7.1. The Al–Mo system

The Al–Mo phase diagram calculated using the re-optimized parameters is shown in Fig. 1(a). The new description is in agreement with the congruent melting of AlMo and the eutectic reaction

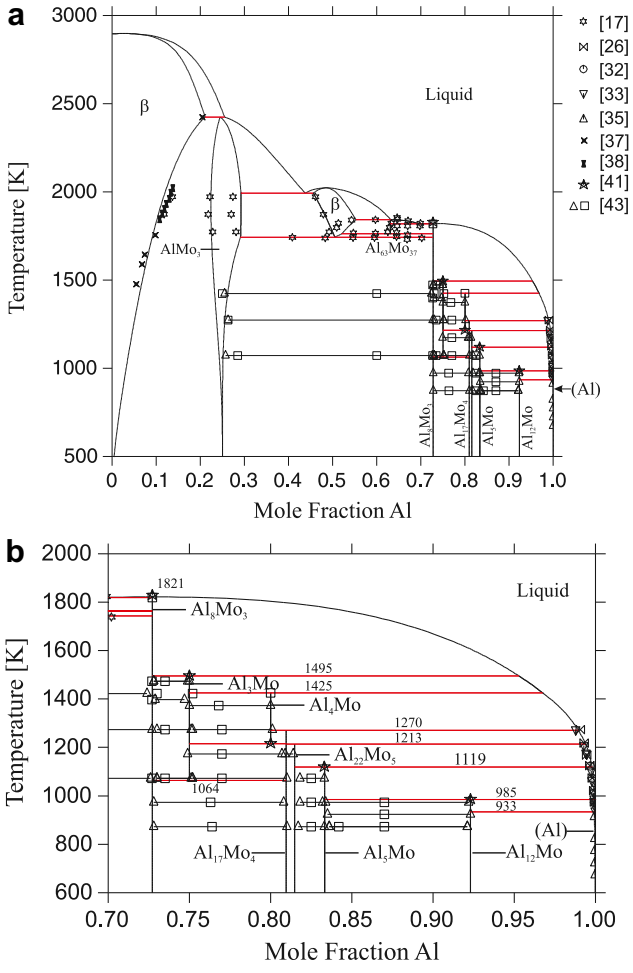

Fig. 1. (A) Full and (B) partial Al–Mo phase diagram calculated using the new description. The experimental data from the literature are superimposed.

between the liquid, δ-$AlMo_3$, and AlMo phases determined by Rexer [17]. The β phase melts congruently at 2023 K, which is in excellent agreement with the critical evaluation of Schuster [42]. The congruent melting of Al_8Mo_3 is calculated at 1821 K, which is in good agreement with the thermal analysis measurements of Schuster and Ipser [41] (1828 ± 10 K) and Eumann et al. [43] (1819 ± 5 K). The partial phase diagram from 70 to 100 at.%Al is shown in Fig. 1(b). All intermetallic phases in the Al–Al_8Mo_3 region are reproduced, and the temperature ranges of stability are in very good agreement with the work of Eumann et al. [43].

The calculated enthalpies of formation of the β phase at 2, 4, 8, and 11 at.%Al, of the AlMo phase, the δ-$AlMo_3$ phase at 25 at.%Mo, and of the Al_8Mo_3 phase from the pure elements are shown in Fig. 2. The experimental data of Shilo and Franzen [38] and Meschel and Kleppa [44] on the enthalpies of formation of the phases are superimposed. While the enthalpies of formation of the Mo-rich β phase, the δ-$AlMo_3$ phase, and the Al_8Mo_3 phase could be well reproduced, the enthalpy of formation of AlMo could not. The present calculation gives a value of -13.2 kJ/mol whereas the work of Shilo and Franzen [38], which used vapor pressure measurements from the Knudsen effusion method, gives a value of -31.3 kJ/mol using the third law method and -27.8 kJ/mol using the second law method. The description of Du et al. [19] is in quite good agreement with the data of Shilo and Franzen [38]. However, the description of Du et al. [19] calculates the peritectic formation of AlMo instead of the congruent melting of AlMo. Both the present description and the description of Du et al. [19] model the β phase with second order Redlich–Kister binary interaction parameters whereas the liquid phase of the present description is modeled with third order Redlich–Kister polynomial parameters and the liquid phase of Du et al. [19] is modeled with second order Redlich–Kister polynomial parameters. This indicates that the enthalpy of formation data of Shilo and Franzen [38] may be inconsistent with the congruent melting of AlMo. Since vapor pressure measurements for the determination of enthalpies of formation are not as reliable as direct reaction calorimetry measurements, the enthalpy of formation of AlMo should be re-investigated using direct reaction calorimetry.

7.2. The Ti–Al–Mo system

The predicted liquidus surface calculated with the new description for the Ti–Al–Mo system is shown in Fig. 3. The temperatures and compositions of the invariant reactions with the liquid phase are given in Table 3 and are compared with the temperatures of the invariant reactions given in the assessment of Tretyachenko [60]. There is a reasonably good agreement between the calculated invariant reaction temperatures and those suggested in the critical evaluation of Tretyachenko [60] although only the parameters for the β, η, and δ phases were re-optimized.

The calculated β solidus is also superimposed on the liquidus surface (Fig. 3). The calculations show that the β solidus is divided into the Al-rich β solidus and the β solidus surrounding the δ phase. This separation occurs because the congruent melting of the AlMo phase in the binary Al–Mo system is reproduced and because the β and AlMo phases are modeled as a single phase. Al–Mo alloys with Al compositions from 45.6 to 55.2 at.%Al, which are the β solidus compositions along the Al–Mo binary, go through a region of single phase β (AlMo) on solidification. When this feature of the Al–Mo phase diagram is extended into the ternary system, the β phase becomes continuous from the Ti–Mo binary to the Al–Mo binary. This is in accordance with the work of Nino et al. [15]. Additionally, since the calculated Al-rich β solidus occurs at Al-compositions which are higher than those of the alloys studied by Nino et al. [15], these alloys are calculated to solidify as single phase β, which is in excellent agreement with the work of Nino et al. [15].

Fig. 4 shows the calculated isothermal section at 1773 K. The alloy of composition 3 at.%Ti–52 at.%Al–45 at.%Mo is calculated in the single phase β field, which is in very good agreement with the experimental work of Nino et al. [15]. The calculated isothermal section at 1673 K is shown in Fig. 5. The results indicate very good agreement with the experimentally determined $\beta + Al_8Mo_3 + \delta$ three phase field at 1673 K of Nino et al. [15]. However, neither the α phase nor the γ phase extends to high enough Mo compositions. For example, Singh and Banerjee [52] reported that an alloy of

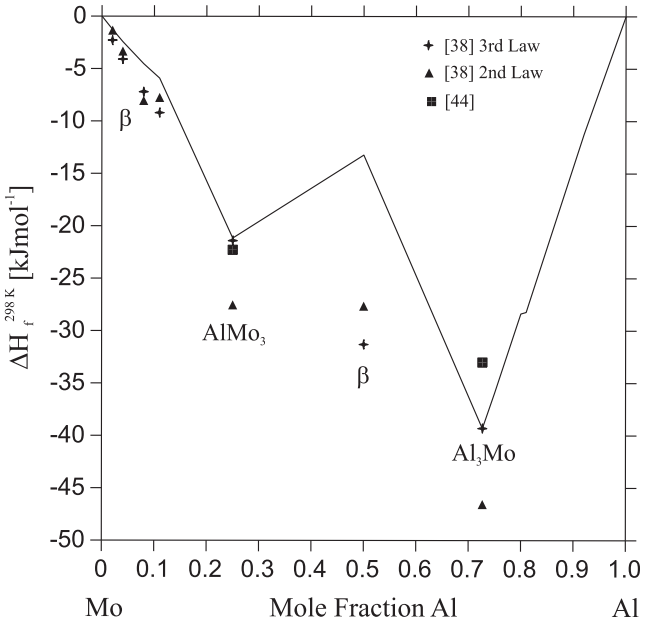

Fig. 2. Calculated and experimentally determined enthalpies of formation of the phases in the Al–Mo system.

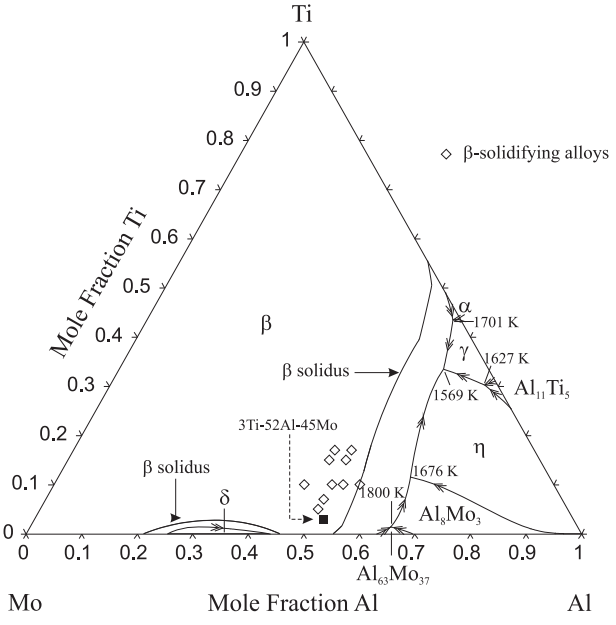

Fig. 3. Liquidus surface calculated with the new description for the Ti–Al–Mo system. All alloys indicated were shown to solidify as single phase β in the work of Nino et al. [15], with which the new liquidus surface is in very good agreement.

Table 3
Invariant reactions with the liquid phase in the Ti–Al–Mo system.

Reaction $\varphi_1+\varphi_2+\varphi_3+\varphi_4$	Temperature [K]	Liquid Composition [at.%]			Reference
		Al	Mo	Ti	
Liquid + $Al_{63}Mo_{37}$ → β + Al_8Mo_3	1800	64.9	33.7	1.4	This work
	~1773	–	–	–	[60]
Liquid + α → β + γ	1701	55.1	1.5	43.5	This work
	~1713	–	–	–	[60]
Liquid + Al_8Mo_3 → β + η	1676	63.4	25.1	11.5	This work
	1743	–	–	–	[60]
Liquid + ζ → η + γ	1627	67.4	2.4	30.2	This work
	~1673	–	–	–	[60]
Liquid → γ + η + β	1569	55.4	8.2	33.4	This work
	1643	–	–	–	[60]
Liquid + Al_8Mo_3 → η + Al_3Mo	1494	95.2	4.7	0.1	This work
Liquid + Al_3Mo → η + Al_4Mo	1425	96.7	3.3	0.0	This work
Liquid + Al_4Mo → η + $Al_{17}Mo_4$	1270	99.4	0.6	0.0	This work
Liquid + $Al_{17}Mo_4$ → η + $Al_{22}Mo_5$	1213	99.8	0.2	0.0	This work
Liquid + $Al_{22}Mo_5$ → η + Al_5Mo	1119	99.8	0.2	0.0	This work
Liquid + η + Al_5Mo → $Al_{12}Mo$	985	99.97	0.03	0.0	This work

composition 50 at.%Ti–48 at.%Al–2 at.%Mo is in the single phase α field at 1673 K but this alloy is calculated in the $\beta+\gamma$ two phase region. Similarly, Singh and Banerjee [52] showed that the maximum composition of Mo in the γ phase at 1673 K is 3 at.%Mo whereas the present calculation shows a maximum composition of Mo in γ of only 0.2 at.% Mo. In fact, while the original Ti–Al–Mo dataset of Saunders [14] shows an acceptable extension of the α and γ phases, the increased stability of the β phase in the present work leads to a retraction of the α and γ phase fields toward the Ti–Al binary. This indicates that the parameters of the α and γ phases should be re-optimized to be able to reproduce the extension of these phases into the ternary system.

The calculated isothermal sections at 1541 and 1539 K shown in Fig. 6(a) and 6), respectively indicate that the solid state transition reaction $\beta+Al_8Mo_3 \rightarrow \delta+\eta$ is calculated to take place at 1540 K. These calculated isothermal sections also show a large extension of the δ phase into the ternary along 25 at.%Al. While this extension has not been confirmed experimentally, it follows from the requirement to fit the composition of the δ phase in the $\beta+Al_8Mo_3+\delta$ tie triangle at 1673 K. However, the extension of the δ phase should be checked by performing more experiments in this region.

The calculated partial isopleth at constant 50 at.%Al with Ti contents from 0 to 20 at.%Ti is shown in Fig. 7 with the experimental results of Nino et al. [15] superimposed. Alloy compositions indicated as filled squares were shown to be single phase β after they were heat treated at the respective temperatures and quenched, and alloy compositions shown as filled circles were found to be two phase $\eta+\delta$. The phase boundary estimated from chemical analysis is shown as a filled diamond whereas all other solid state transformation temperatures measured using thermal analysis are indicated as triangles. The calculated isopleth is in very good agreement with the transformation temperatures from Nino et al. [15] shown as filled triangles but deviates from the transformation temperatures suggested by Nino et al. [15] shown as

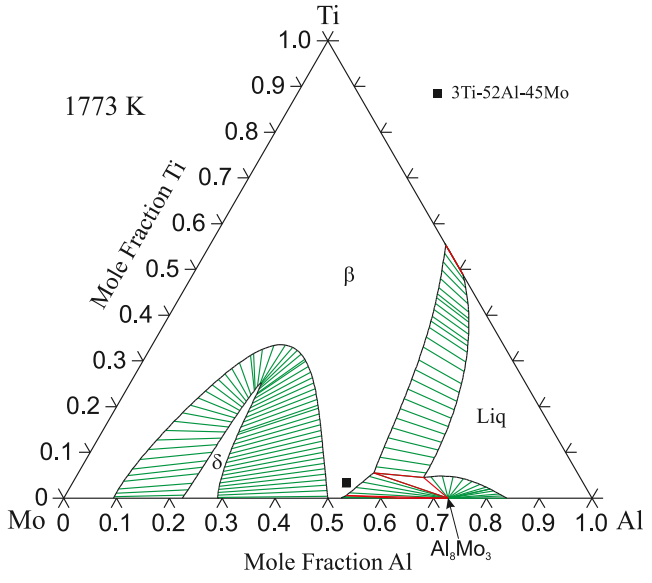

Fig. 4. Isothermal section at 1773 K calculated using the new description for the Ti–Al–Mo system.

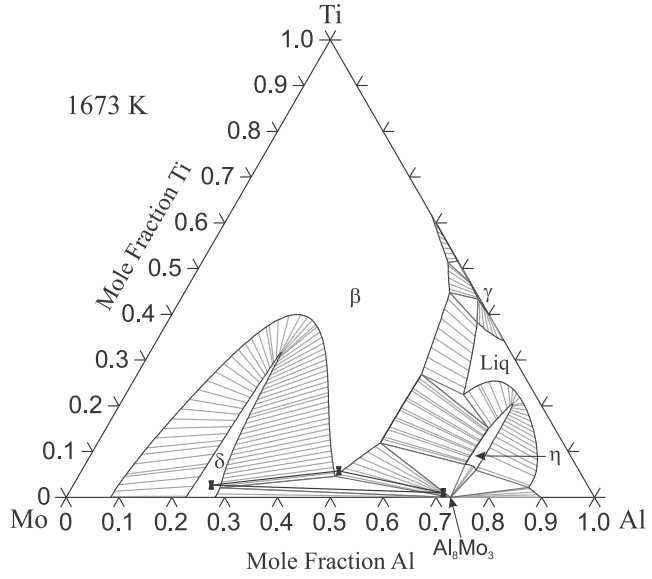

Fig. 5. Isothermal section at 1673 K calculated using the new description for the Ti–Al–Mo system. The compositions of the phases in the $\beta+Al_8Mo_3+\delta$ three phase triangle determined by Nino et al. [15] are included.

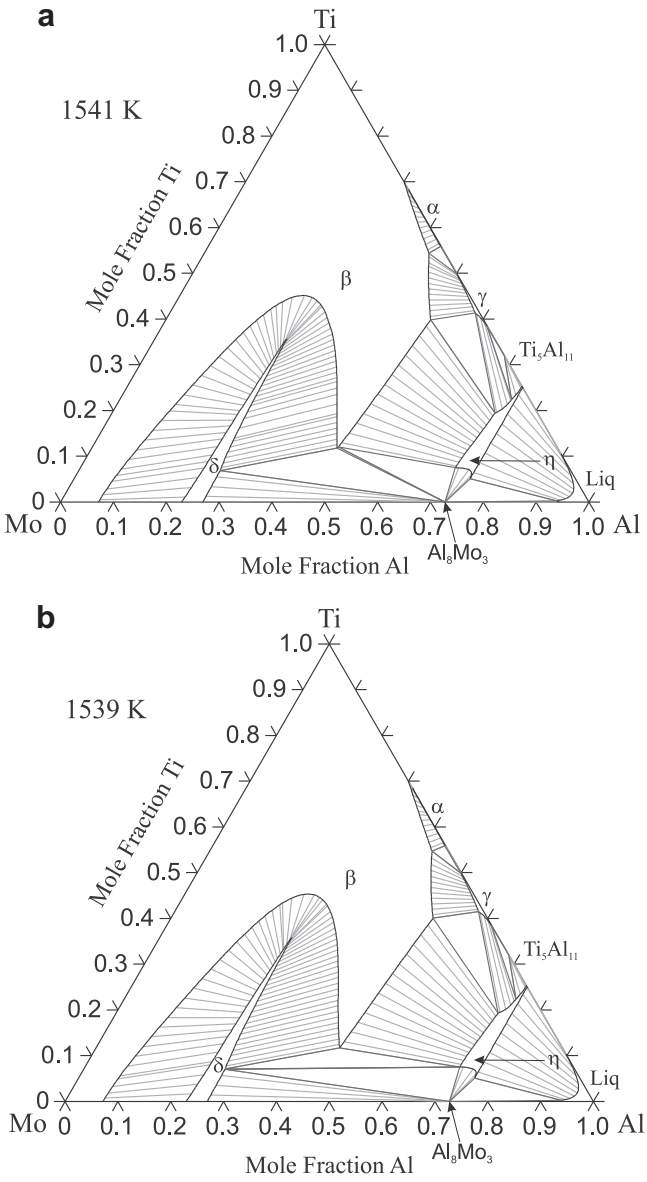

Fig. 6. Isothermal sections at (A) 1541 K and (B) 1539 K calculated using the new description for the Ti–Al–Mo system. The transition reaction $\beta + Al_8Mo_3 \rightarrow \delta + \eta$ takes place at 1540 K.

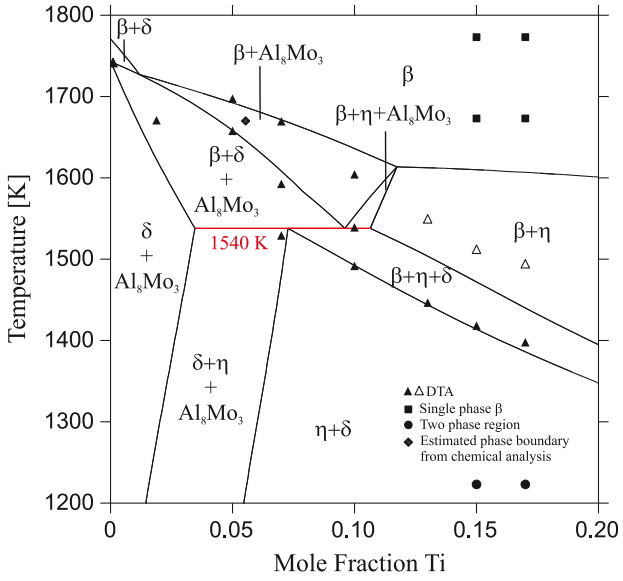

Fig. 7. Isopleth calculated through 50 at.%Al. The experimental data from Nino et al. [15] are included.

open triangles. This deviation may, however, result from the kind of DTA curve interpretation implemented by Nino et al. [15]. Specifically, the DTA curves for alloys with 13, 15, and 17 at.%Ti showed broad peaks on heating at temperatures higher than 1400 K. The filled triangles then represent temperatures corresponding to the first deviation of the DTA heat flow signals from the baseline on heating whereas the open triangles represent temperatures corresponding to the return of the DTA heat flow signal to the baseline. While the first deviation from baseline may be associated with a phase transformation, the return to baseline usually only corresponds to the completion of the phase transformation. Therefore, while it is possible that the broad DTA peaks recorded by Nino et al. [15] correspond to multiple phase transformations, the key data which can be used for phase diagram determination are the temperatures at which the first phase transformation takes place, shown as the filled triangles. The open triangles are included in Fig. 7 to show the complete work of Nino et al. [15]. It must also be noted that the original work of Nino et al. [15] associates the open triangles with the $\beta + \eta \rightarrow \beta$ phase transformation. While this transformation is expected to occur, it is equally possible that this transformation occurs at the higher temperatures indicated by the calculated isopleth. The only evidence of such a phase transformation from the work of Nino et al. [15] is the microstructure of the alloy 15 at.%Ti–50 at.%Al–35 at.%Mo which was slow cooled to 1323 K at various cooling rates from 30 K/min to 5 K/min. However, heat treating and quench experiments to ascertain the temperature range of this phase transformation combined with DTA experiments of samples equilibrated at temperatures just before the expected transformation temperature were not performed.

While there is evidence that a ternary σ phase with stoichiometry $Ti_{1.5}Al_2Mo_{1.5}$ [48] exists, this phase was not modeled in this work. However, this should not affect the calculated isothermal sections presented, as the σ phase forms at $\approx$1523 K [60] and the lowest temperature calculated isothermal section which is shown is the isothermal section at 1540 K. However, the presence of the ternary σ phase should affect the calculated partial isopleth at temperatures below 1523 K. It is possible that with the inclusion of the σ phase as a stoichiometric phase, the two phase $\sigma + \beta$ field which forms could intersect the $\beta + \delta$ two phase field to produce a $\beta + \delta + \sigma$ field with a Ti-rich β phase and a $\beta + \delta + \sigma$ field with a Ti-poor β phase. Likewise, it is possible that the $\sigma + \beta$ region also intersects the $\beta + \eta$ two phase region to produce a $\beta + \eta + \sigma$ three phase field with a Ti-rich β phase and a $\beta + \eta + \sigma$ three phase field with a Ti-poor β phase. The $\beta + \delta + \sigma$ and $\beta + \eta + \sigma$ three phase fields formed with a Ti-rich β phase are shown in the critically evaluated 1273 K isothermal section of Tretyachenko [60]. However, the $\beta + \delta + \sigma$ and $\beta + \eta + \sigma$ three phase fields formed with Ti-poor β phase are not indicated. It is possible that these two three phase regions participate in a transition reaction to produce the $\delta + \eta + \sigma$ and $\delta + \eta + \beta$ fields. The $\delta + \eta + \sigma$ three phase field is indicated in the critically evaluated 1198 K isothermal section of Tretyachenko [60], but the $\delta + \eta + \beta$ field with a Ti-poor, isolated β phase field is not. More experimental work should be conducted to clarify the phase equilibria in this region.

8. Conclusion

Thermodynamic descriptions for the Al–Mo system and for the Ti–Al–Mo system reproducing phase equilibria data from 0 to

20 at.%Ti were developed. The new Al–Mo description models the Mo-rich β phase and the AlMo phase as a single phase, reproduces the congruent melting of the AlMo phase, and calculates an eutectic reaction between the liquid, AlMo, and δ-$AlMo_3$ phases at 1993 K. The calculated Al–Mo phase diagram is in excellent agreement with the work of Rexer [17] in the Mo-rich region and with the work of Eumann [43] in the Al-rich region. The new Al–Mo binary description was used for the desciption of the Ti–Al–Mo system. The reoptimized dataset for the Ti–Al–Mo system is in good agreement with the work of Nino et al. [15] which shows the continuity of the β phase from the Ti–Mo binary to the Al–Mo binary, the presence of the single phase β field for several Ti-poor alloys, and the invariant reaction $\beta + Al_8Mo_3 \rightarrow \delta + \eta$ at 1540 K.

Acknowledgments

This research was supported by NSF/AFOSR under Grant No. DMR-0605702 and DMR-0856622.

Appendix A. Thermodynamic dataset for the Ti–Al–Mo system.

Parameter	Function	Reference
β: (Al, Nb, Ti)		
G^{β}_{Al}	$GBCC_{Al}$	[14]
G^{β}_{Mo}	$GHSER_{Mo}$	[14]
G^{β}_{Ti}	$GBCC_{Ti}$	[14]
${}^0L^{\beta}_{Al,Mo}$	$-73{,}113.2883 + 22.7704371\,T$	This work
${}^1L^{\beta}_{Al,Mo}$	$-16{,}584.5446$	This work
${}^2L^{\beta}_{Al,Mo}$	$-18{,}877.1914$	This work
${}^0L^{\beta}_{Al,Ti}$	$-128{,}500 + 39\,T$	[14]
${}^1L^{\beta}_{Al,Ti}$	6000	[14]
${}^2L^{\beta}_{Al,Ti}$	21,200	[14]
${}^0L^{\beta}_{Mo,Ti}$	2000	[14]
${}^1L^{\beta}_{Mo,Ti}$	-2000	[14]
${}^0L^{\beta}_{Al,Mo,Ti}$	$-34{,}665.3396 - 62.7530956\,T$	This work
${}^1L^{\beta}_{Al,Mo,Ti}$	$-436{,}018.268 + 199.763999\,T$	This work
${}^2L^{\beta}_{Al,Mo,Ti}$	$701{,}116.243 - 457.111853\,T$	This work
η: (Al, Nb, Ti)$_3$(Al, Nb, Ti)		
$G^{\eta}_{Al:Al}$	$4\cdot GHSER_{Al} + 80{,}000$	This work
$G^{\eta}_{Mo:Al}$	$3\cdot GFCC_{Mo} + GHSER_{Al} + 80{,}000$	This work
$G^{\eta}_{Ti:Al}$	$3\cdot GHSER_{Ti} + GHSER_{Al} + 304{,}592 - 37.024\,T$	[14]
$G^{\eta}_{Al:Mo}$	$3\cdot GHSER_{Al} + GHSER_{Mo} - 138{,}710.769 + 40.9417405\,T$	This work
$G^{\eta}_{Mo:Mo}$	$4\cdot GFCC_{Mo} + 80{,}000$	[14]
$G^{\eta}_{Ti:Mo}$	$3\cdot GFCC_{Ti} + GFCC_{Mo}$	[14]
$G^{\eta}_{Al:Ti}$	$3\cdot GHSER_{Al} + GHSER_{Ti} - 144{,}592 + 37.024\,T$	[14]
$G^{\eta}_{Mo:Ti}$	$3\cdot GFCC_{Mo} + GFCC_{Ti}$	[14]
$G^{\eta}_{Ti:Ti}$	$4\cdot GHSER_{Ti} + 80{,}000$	[14]
${}^0L^{\eta}_{Al,Mo:Mo}$	$-80{,}000$	[14]
${}^0L^{\eta}_{Al,Mo:Ti}$	$-80{,}000$	This work
${}^0L^{\beta}_{Al,Ti:Ti}$	$-60{,}000$	[14]
${}^0L^{\eta}_{Al,Ti:Mo}$	$-60{,}000$	This work
${}^0L^{\eta}_{Al:Mo,Ti}$	$-238{,}049.751 + 120.0\,T$	This work
δ: (Al, Mo, Ti)$_{0.75}$(Al, Mo, Ti)$_{0.25}$		
$G^{\delta}_{Al:Al}$	$GHSER_{Al} + 10{,}000$	This work
$G^{\delta}_{Mo:Al}$	$0.75\cdot GHSER_{Al} + 0.25\cdot GHSER_{Mo} - 21{,}180.9741 + 3.3394361\,T$	This work
$G^{\delta}_{Ti:Al}$	$0.75\cdot GHSER_{Ti} + 0.25\cdot GHSER_{Al} - 22{,}250 + 5.6\,T$	[14]
$G^{\delta}_{Al:Mo}$	$0.75\cdot GHSER_{Al} + 0.25\cdot GHSER_{Mo} + 10{,}000$	This work
$G^{\delta}_{Mo:Mo}$	$GHSER_{Mo} + 10{,}000$	This work
$G^{\delta}_{Ti:Mo}$	$0.75\cdot GHSER_{Ti} + 0.25\cdot GHSER_{Mo} + 10{,}000$	[14]
$G^{\delta}_{Al:Ti}$	$0.75\cdot GHSER_{Al} + 0.25\cdot GHSER_{Ti} + 10{,}000$	This work
$G^{\delta}_{Mo:Ti}$	$0.75\cdot GHSER_{Mo} + 0.25\cdot GHSER_{Ti} + 10{,}000$	This work
$G^{\delta}_{Ti:Ti}$	$GHSER_{Ti} + 10{,}000$	This work
${}^0L^{\beta}_{Al,Mo:Al}$	$0.455738495\,T$	This work
${}^0L^{\beta}_{Mo:Al,Mo}$	$-2.63250337\,T$	This work
${}^0L^{\beta}_{Mo,Ti:Al}$	$-22{,}021.7991\,T$	This work
(Al): (Al, Nb, Ti)		
$G^{(Al)}_{Al}$	$GHSER_{Al}$	[14]
$G^{(Al)}_{Mo}$	$GFCC_{Mo}$	[14]
$G^{(Al)}_{Ti}$	$GHSER_{Ti} + 6000 - 0.1\,T$	[14]
${}^0L^{(Al)}_{Al,\,Mo}$	$-146{,}174.503 + 75.6992933\,T$	This work
${}^0L^{(Al)}_{Al,Ti}$	$-128{,}970 + 39\,T$	[14]
${}^1L^{(Al)}_{Al,Ti}$	-5000	[14]
${}^2L^{(Al)}_{Al,Ti}$	20,000	[14]
${}^0L^{(Al)}_{Al,Ti}$	16,500	[14]
Liq: (Al, Nb, Ti)		
G^{Liq}_{Al}	$GLIQ_{Al}$	[14]
G^{Liq}_{Mo}	$GLIQ_{Mo}$	[14]
G^{Liq}_{Ti}	$GLIQ_{Ti}$	[14]
${}^0L^{Liq}_{Al,Mo}$	$-148{,}756.738 + 60.614292\,T$	This work
${}^1L^{Liq}_{Al,Mo}$	$84{,}284.5911 - 26.0603279\,T$	This work
${}^2L^{Liq}_{Al,Mo}$	$-96{,}206.0414 + 26.5383283\,T$	This work
${}^3L^{Liq}_{Al,Mo}$	$55{,}040.9600 - 23.0458461\,T$	This work
${}^0L^{Liq}_{Al,Ti}$	$-108{,}250 + 38\,T$	[14]
${}^1L^{Liq}_{Al,Ti}$	$-6000 + 5\,T$	[14]
${}^2L^{Liq}_{Al,Ti}$	15,000	[14]
${}^0L^{Liq}_{Al,Ti}$	$-9000 + 2\,T$	[14]
${}^0L^{Liq}_{Al,Mo,Ti}$	$-100{,}000$	[14]
${}^1L^{Liq}_{Al,Mo,Ti}$	$-100{,}000$	[14]
${}^2L^{Liq}_{Al,Mo,Ti}$	$-100{,}000$	[14]
$Al_{63}Mo_{37}$: $(Al)_{63}(Mo)_{37}$		
$G^{Al_{63}Mo_{37}}$Al : Mo	$63\cdot GHSER_{Al} + 37\cdot GHSER_{Mo} - 1{,}901{,}739.23 + 43.1008259\,T$	This work
Al_8Mo_3: $(Al)_8(Mo)_3$		
$G^{Al_8Mo_3}$Al : Mo	$8\cdot GHSER_{Al} + 3\cdot GHSER_{Mo} - 432{,}300 + 128.341056\,T$	This work
Al_3Mo: $(Al)_3(Mo)$		
G^{Al_3Mo}Al : Mo	$3\cdot GHSER_{Al} + GHSER_{Mo} - 143{,}710.769 + 40.9417405\,T$	This work
Al_4Mo: $(Al)_4(Mo)$		
G^{Al_4Mo}Al : Mo	$4\cdot GHSER_{Al} + GHSER_{Mo} - 141{,}877.438 + 35.4373736\,T$	This work
$Al_{17}Mo_4$: $(Al)_{17}(Mo)_4$		
$G^{Al_{17}Mo_4}$Al : Mo	$17\cdot GHSER_{Al} + 4\cdot GHSER_{Mo} - 592{,}950.517 + 158.690172\,T$	This work
$Al_{22}Mo_5$: $(Al)_{22}(Mo)_5$		
$G^{Al_{22}Mo_5}$Al : Mo	$22\cdot GHSER_{Al} + 5\cdot GHSER_{Mo} - 740{,}721.623 + 195.980411\,T$	This work
Al_5Mo: $(Al)_5(Mo)$		
G^{Al_5Mo}Al : Mo	$5\cdot GHSER_{Al} + GHSER_{Mo} - 147{,}852.738 + 37.7948482\,T$	This work
$Al_{12}Mo$: $(Al)_{12}(Mo)$		
$G^{Al_{12}Mo}$Al : Mo	$12\cdot GHSER_{Al} + GHSER_{Mo} - 146{,}292.986 + 32\,T$	This work

References

[1] Liu CT. Review: recent advances in ordered intermetallics. Mat Chem Phys 1995;42:77–86.
[2] Liu CT, Schneibel JH, Maziasz PJ, Wright JL, Easton DS. Tensile properties and fracture toughness of TiAl alloys with controlled microstructures. Intermetallics 1996;4:429–40.

[3] Morris MA, Li YG, Leboeuf M. Variation of the phase distribution in a Ti–44Al–2Mo alloy by annealing: influence on its strength and ductility. Scr Metall Mater 1994;31:449–54.
[4] Kishida K, Johnson DR, Masuda Y, Umedaa H, Inui H, Yamaguchi M. Deformation and fracture of PST crystals and directionally solidified ingots of TiAl–based alloys. Intermetallics 1998;6:679–83.
[5] Kim SW, Lee HN, Oh MH, Wee DM. Effects of the variation in α–phase volume fraction on the thermal stability of TiAl alloys with a lamellar microstructure. J Mater Sci 2004;39:6929–35.
[6] Ebrahimi F, Hoelzer DT, Castillo-Gomez JR. Fracture toughness of σ+x microstructures in the Nb–Ti–Al system. Mat Sci Eng A 1993;171:35–45.
[7] d'Aragao BJG, Ebrahimi F. High temperature deformation of Nb–Ti–Al alloys with $\sigma + \gamma$ microstructure. Mat Sci Eng A 1996;208:37–46.
[8] Yu TH, Koo CH. Phase characterization of a hot-rolled Ti–40Al–10Nb alloy at 1000 to 1200 °C. Acta Metall 1998;39:915–22.
[9] Sun FS, Cao CX, Kim SE, Lee YT, Yan MG. Alloying mechanism of beta stabilizers in a TiAl alloy. Metall Mater Trans 2001;32A(7):1573–89.
[10] Yang CT, Lu YC, Koo CH. The high temperature tensile properties and microstructural analysis of Ti–40Al–15Nb alloy. Intermetallics 2002;10:161–9.
[11] Xu XJ, Xu LH, Lin JP, Wang YL, Lin Z, Chen GL. Pilot processing and microstructure control of high Nb containing TiAl alloy. Intermetallics 2005;13:337–41.
[12] Das S, Mishurda JC, Allen WP, Perepezko JH, Chumbley LS. Development of a $(\gamma + \beta_0)$ lamellar microstructure in a $Ti_{45}Al_{50}Mo_5$ alloy. Scr Metall Mater 1993;28:489–94.
[13] Jung IS, Jang HS, Oh MH, Lee JH, Wee DM. Microstructure control of TiAl alloys containing β stabilizers by directional solidification. Mat. Sci. Eng. A 2002;329–331:13–8.
[14] Saunders N. In: Ansara I, editor. COST 507, thermochemical database for light elements. European Commission; 1994.
[15] Nino R, Fujinaka J, Shimamura H, Miura S, Mohri T. Phase equilibria and microstructure evolution of Al–Mo–Ti alloys. Intermetallics 2003;11:611–23.
[16] Cupid DM. Thermodynamic assessment of the Ti–Al–Nb, Ti–Al–Cr, and Ti–Al–Mo systems. Ph.D. thesis, University of Florida; 2009.
[17] Rexer J. Die Phasengleichgewichte im System Aluminum–Molybdän bei Temperaturen oberhalb 1400 °C. Z Metallkd 1971;62:844–8.
[18] Saunders N. The Al–Mo system (aluminum–molybdenum). J Phase Equilib 1997;18:370–8.
[19] Du Z, Guo C, Li C, Zhang W. Thermodynamic description of the Al–Mo and Al–Fe–Mo systems. J Phase Equilib Diffus 2009;30:487–501.
[20] Adam J, Rich JB. The crystal structure of WAl_{12}, $MoAl_{12}$ and (Mn, Cr)Al_{12}. Acta Cryst 1954;7:813–6.
[21] Walford LK. The structures of the intermetallic phases $MoAl_{12}$, $ReAl_{12}$, and $TcAl_{12}$. Acta Cryst 1964;17:57–9.
[22] Sperner F. Das Zweistoffsystem Aluminum-Molybdän. Z Metallkd 1959;50:588–91.
[23] Clare JWH. Compounds present in aluminum-rich alloys of the aluminum-molybdenum system. J Inst Metals 1960;89:232–4.
[24] Pötzschke M, Schubert K. Zum Aufbau einiger zu T^4–B^3 homologer und quasihomologer Systeme. Z Metallkd 1962;53:548–59.
[25] Kamei K, Ninomiya T, Terauchi S. Aluminum–molybdenum binary phase diagram. Technol Rept Kansai Univ 1972;13:93–106.
[26] Yamaguchi K, Simizu K. The equilibrium diagram of the Al–Mo system. Nippon Kinzoku Gakkaishi 1940;4:390–2.
[27] Wöhler F, Michel F. Über krystallisirte Verbindungen von Aluminium mit Metallen. Liebigs Ann Chem Pharm 1860;115:102–5.
[28] Reimann H. Untersuchungen über Aluminum–Molybdänlegierungen. Z Metallkd 1922;14:119–23.
[29] Leake JA. The refinement of the crystal structure of the intermetallic phase Al_4Mo. Acta Cryst 1964;17:918–24.
[30] Forsyth JB, Gran G. The structure of the intermetallic phase γ (Mo–Al)–Mo_3Al_8. Acta Cryst 1962;15:100–4.
[31] Tenderloo GV, Landuyt JV, Amelinckx S. The defect structure of aluminum rich Al–Mo alloys. Mat Res Bull 1975;10:941–8.
[32] Yeremenko V, Natanzon YV, Dybkov VI. Interactions of the refractory metals with liquid alloy. J Less Commons Metals 1976;50:29–48.
[33] Malinovskii RR. Position of the liquidus in the Al–Mo system. Tekhnol Legk Splavov 1980;1:60–1.
[34] Röntgen P, Koch W. Einfluss von Schwermetallen auf Aluminumlegierungen. Z Metallkd 1933;25:182–5.
[35] Vigdorovich VN, Glazov VM, Glagoleva NN. An investigation of the solubility of Cr, Mo, and W in Al by the microhardness method. Izv VUZ Tsvetnaya Met 1960;2:143–6.
[36] Tech. rep. Ham JL. 1st Annual report on project nr 031-331. Climax Molybdenum Company; 1950
[37] Ham JL, Herzig AJ. 2nd Annual report on project nr 031-331. Tech. rep.. Climax Molybdenum Company; 1951
[38] Shilo I, Franzen HF. High temperature thermodynamic study of the molybdenum-rich regions of the Mo–Al system. J Electrochem Soc 1982;129:2613–7.
[39] Brewer L, Lamoreaux RH, Ferro R, Marazza R. The Al–Mo system (aluminium–molybdenum). Bull. Alloy Phase Diag 1980;1:71–5.
[40] Walford LK. The phase diagram of the Al–Mo system. Philos Mag 1964;9:513–6.
[41] Schuster JC, Ipser H. The Al–Al_8Mo_3 section of the binary system aluminum–molybdenum. Metall Trans A 1991;22:1729–36.
[42] Schuster JC. Al–Mo (aluminium–molybdenum). In: Effenberg G, editor. MSIT binary evaluation program. Stuttgart: MSIT workplace, MSI, Materials Science International Services GmbH; 2003. Document ID: 20.12123.1.20.
[43] Eumann M, Sauthoff G, Palm M. Re-evaluation of phase equilibria in the Al–Mo system. Int J Mater Res 2006;97:1502–11.
[44] Meschel SV, Kleppa OJ. Standard enthalpies of formation of 4d aluminides by direct synthesis calorimetry. J Alloys Compd 1993;191:111–6.
[45] Sudavtsova VS, Batalin GI, Tutevich VS. Thermodynamic properties of molten binary alloys in systems Al–(Zr, Nb, Mo). Russ Metall 1985;5:183–5.
[46] Dinsdale AT. NPL report DMA(A) 195; 1989.
[47] Dinsdale AT. SGTE data for pure elements. CALPHAD 1991;15:317–425.
[48] Hansen RC, Raman A. Alloy chemistry of σ (β–U)-related phases III. σ-Phases with non-transition elements. Z Metallkd 1970;61:115–20.
[49] Eremenko VN, Sukhaya SA, Tretyachenko LA. Isothermal section of the Ti–Al–Mo phase diagram at 1300 °C. Stabil i Metastabil Fazy v Mater; 1987:106–14.
[50] Abdel-Hamid AA. Crystallization of complex aluminide compounds from dilute Al–Ti melts containing one or two other transition metals of IVB to VIB groups. Z Metallkd 1990;81:601–5.
[51] Kimura M, Hashimoto K. High-temperature phase equilibria in the Ti–Al–Mo system. J Phase Equilib 1999;20:224–30.
[52] Singh AK, Banerjee D. Transformations in the $\alpha_2 + \gamma$ titanium aluminide alloys containing molybdenum: part II. Heat treatment. Metall Mater Trans A 1997;28:1745–53.
[53] Eremenko VN, Tretyachenko LA, Sukhaya LA, Petukh VM. Investigation of the structure of alloys of the Ti–Mo–Al system. Akad Nauk Ukr; 1990:83–135.
[54] Banerjee D, Krishnan RV, Vasu KI. A reconsideration of phase relations in the Ti–Al–Mo and Ti–Al systems. Metall Trans A 1980;11:1095–105.
[55] Margolin H. Metals handbook. Metals Park, Ohio: ASM; 1973.
[56] Schuster JC, Palm M. Reassessment of the binary aluminum–titanium phase diagram. J Phase Equilib Diffus 2006;27:255–77.
[57] Das S, Jewett T, Perepezko J. In: Darolia R, Lewandowski JJ, Liu CT, Martin PL, Miracle DB, Nathal MV, editors. Structural intermetallics. The Minerals, Metals, and Materials Society; 1993.
[58] Böhm H, Löhberg K. Über eine Überstrukturphase vom CsCl-Typ im System Titan–Molybdän–Aluminium. Z. Metallkd. 1958;49:173–8.
[59] Singh AK, Kumar S, Banumathy S, Mandal RK. Structure of the B2 phase in Ti–25Al–25Mo alloy. Phil Mag 2007;87:5435–45.
[60] Tretyachenko L. Aluminium–molybdenum–titanium. In: Martienssen W, editor. Landolt–Boernstein new series numerical data and functional relationships in science and technology. Ternary alloy systems: phase diagrams, crystallographic and thermodynamic data critically evaluated by MSIT, Group IV, vol. II. Berlin, Heidelberg: Springer-Verlag; 2005. p. 287–316. Subvolume A, Part 3.
[61] Budberg P, Schmid-Fetzer R. Aluminium–molybdenum–titanium. In: Effenberg G, editor. MSIT ternary evaluation program. Stuttgart: MSIT workplace, MSI, Materials Science International Services GmbH; 1993. Document ID: 10.17143.1.20.
[62] Raghavan V. Al-Mo-Ti (aluminium–molybdenum–titanium). J Phase Equilib Diffus 2005;26:357–9.
[63] Schmid-Fetzer R. Al–Ti (aluminium–titanium). In: Effenberg G, editor. MSIT binary evaluation program. Stuttgart: MSIT workplace, MSI, Materials Science International Services GmbH; 2003. Document ID: 20.15634.1.20.
[64] Raghavan V. Al–Ti (aluminum–titanium). J Phase Equilib Diffus 2005;26:171–2.
[65] Massalski TB. Binary alloy phase diagrams. Metals Park, Ohio: ASM International; 1990.
[66] Redlich O, Kister AT. Algebraic representation of thermodynamic properties and the classification of solutions. Ind Eng Chem 1948;40:345–8.
[67] Hillert M. Empirical methods of predicting and representing thermodynamic properties of ternary solutions. CALPHAD 1980;4:1–12.
[68] Hillert M. The compound energy formalism. J Alloys Compd 2001;320:161–76.
[69] Saunders N, Miodwnik P. In: Cahn RW, editor. CALPHAD (calculation of phase diagrams): a comprehensive guide. Pergamon; 1998.
[70] Lukas HL, Fries SG, Sundman B. The CALPHAD method. Cambridge: Cambridge University Press; 2007.
[71] Jansson B. Ph.D. thesis, Royal Institute of Technology, Stockholm; 1983.
[72] Andersson JO, Helander T, Höglund L, Shi P, Sundman B. THERMO–CALC and DICTRA, computational tools for materials science. CALPHAD 2002;26:273–312.
[73] Chen SL, Daniel S, Zhang F, Chang YA, Yan XY, Xie FY, Schmid-Fetzer R, Oates WA. The PANDAT software package and its applications. CALPHAD 2002;26:175–88.